Flowability characterization and enhancement of aluminium powders for additive manufacturing

Stéphane Touzé, Matthieu Rauch, J.-Y. Hascoët

Flowability characterization and enhancement of aluminium powders for Additive Manufacturing

S. Touzé[1,a], M. Rauch[1,b], J.-Y. Hascoët[1,c]

[1] *Institut de Recherche en Génie Civil et Mécanique (GeM), UMR CNRS 6183*
Ecole Centrale de Nantes, 1 rue de la Noë, 44321 Nantes, France

[a] stephane.touze@ec-nantes.fr, [b] matthieu.rauch@ec-nantes.fr, [c] jean-yves.hascoet@ec-nantes.fr

Abstract

The present work aims at quantifying and enhancing the flowability of cohesive metal powders, in particular aluminium powders, for their use in Additive Manufacturing processes such as Laser Metal Deposition. A flowability criterion, the population-dependent granular Bond number, is calculated for various metal powder samples, which are then tested with a funnel flowmeter under vibrational assistance. It is demonstrated that vibrations at a specific frequency can help trigger and sustain the flow of cohesive metal powders. Another way of enhancing powder flowability is achieved through heat treatment. A significant improvement in flowability is measured for a specific time-temperature setting, thereby enabling the use of a cohesive Al-Cu powder with the Laser Metal Deposition process.

Keywords : Additive Manufacturing, Laser Metal Deposition, Aluminium alloys, Powder Flowability

Nomenclature

Bo_g	Granular Bond number
F_a	Adhesion force
W	Particle Weight
σ	Standard deviation of particle distribution
μ	Mean of particle distribution
d_{50}	Median diameter of particle distribution
d_{10}	10% intercept of cumulative mass distribution over particle diameters
Bo_g^*	Population-dependent Granular Bond number
w_{kl}	Weighing coefficient for interaction probability of particles in two bins *k* and *l* of a discretized particle distribution
$Bo_{g,kl}$	Population-dependent Granular Bond number of particles in two different bins *k* and *l* of a discretized particle distribution
$F_{a,kl}$	Interaction force between particles of bins *k* and *l* of a discretized particle distribution
W_{kl}	Combined weight of interacting particles in two bins *k* and *l* of a discretized particle distribution
$Bo_{g,ref}^*$	Population-dependent Granular Bond number of Reference powder
$Bo_{g,rel}^*$	Relative population-dependent Granular Bond number
$F_{vdW_{ij}}$	Van der Waals force between two particles *i* and *j*
A_{ij}	Hamaker constant for two particles *i* and *j*
R_i	Radius of particle *i*
r_{iS}, r_{iL}	Radius of small-scale (S) and large-scale (L) roughness of particle *i*
y_{iS}, y_{iL}	Height of small-scale (S) and large-scale (L) roughness of particle *i*

D	Interparticle distance
rms_{iL}	Root-Mean-Square of large-scale roughness of particle i
λ_{iL}	Wavelength of large-scale roughness of particle i
F_{cap}	Capillary interaction force
σ_{cap}	Surface tension of capillary bridge
$\overline{\rho_l}$	Molar density of capillary bridge
T	Ambient temperature
R_g	Universal gas constant (molar)
RH	Relative Humidity
Δp_l	Pressure difference over capillary bridge

1. Introduction

Several Metal Additive Manufacturing (AM) processes use gas atomized powders as a raw material, including Selective Laser Melting (SLM) and Laser Metal Deposition (LMD). The LMD process in particular is a flexible AM process that can be used for direct fabrication (Kerninon et al. 2008), Functionally Graded Materials (Muller et al. 2013) and part repairs (Hascoët et al. 2018; Touzé et al. 2018). However, it is highly sensitive to process parameters such as powder flowrate as it requires a continuous, uniform flow of powder material through the LMD nozzle, which is only possible when a powder presents sufficient flowability (Touzé et al. 2019). This so-called flowability of metal powders, which is here defined as the capacity of powder particles to move in bulk by gravity and without a carrier gas, is a key aspect of their overall AM processability. Indeed, in SLM, the powder must be easily spread out by a rake, blade or roller over the powder bed, while also presenting a sufficient packing density to avoid defects in the deposited layers (Aboulkhair et al. 2014; Tan et al. 2017; Vock et al. 2019). In the case of LMD, the powder at rest must be able to flow down a reservoir by gravity before its pneumatic transport towards the LMD nozzle, but there are no constraints on packing density since the powder is directly brought as needed in the deposition zone. Despite the importance of flowability as a powder characteristic for AM processing, there is relatively little published data on powder flowability for LMD, as the focus has mostly been directed onto powder bed processes, for which there is a compromise on flowability due to packing density requirements (Vock et al. 2019).

Some gas atomized metal powders exhibit poor in-process flowability, hereby limiting their use with AM processes such as LMD. This is particularly salient in the case of aluminium powders as they present a relatively low density so that contact and adhesion forces between particles are more prevalent than the force of gravity. Moreover, some of these metal powder particles present imperfections such as satellites formed during the atomization process that effectively produces particle agglomerates that are irregularly shaped, which further hinders powder flowability due to mechanical interlocking forces (Shah et al. 2017). The limited processability of such cohesive powders is difficult to characterize experimentally as the usual methods for powder flowability measurements are ill-suited for cohesive powders. For instance, cohesive powders do not flow through a typical Hall or Carney flowmeter, so that the flowing time or avalanche angle of the powder that has gone through the funnel cannot be evaluated. Measurement methods based on shear cells typically induce powder compaction levels that far exceed the conditions encountered during AM processing, and are thus not very representative of the in-process flowability. Finally, the repeatability of

flowability measurements is typically rather poor with highly cohesive powder.

This paper is organized as follows. Section 2 presents an improvement on a dimensionless flowability criteria, the population-dependent granular Bond number, and its calculation for a number of powder samples. This helps to form a theoretical basis for the bulk behavior of sample powders in terms of flowability. The calculated results are then compared to experimental flowability measurements. Section 3 introduces the use of vibrational excitations at a specific frequency to improve the flowability of cohesive powders. This allows comparing the flowability of powders with wide differences in cohesiveness by using the same experimental setup. It also shows that vibrational excitations at the correct frequency can be used to significantly improve powder flowability. The experimental flowability results for cohesive and non-cohesive powders are then correlated to the flowability criteria calculated for each powder sample. Section 4 demonstrates that a particular heat treatment also provides a significant enhancement in flowability for the considered aluminium powders. The mechanism for flowability enhancement due to heat treatment is then discussed. Finally, section 5 shows LMD deposits of the cohesive aluminium powders under study, thereby demonstrating their use for LMD processing thanks to flowability enhancement techniques.

2. Interparticle forces & Flowability criterion

a. Population-dependent Granular Bond number

The bulk behavior of powder particles is essentially dictated by interaction forces between particles, in particular contact forces such as rolling and sliding friction and adhesion forces such as van der Waals and capillary forces (Castellanos 2005; Shah et al. 2017). Electrostatic forces may also arise if charged particles are present, for example through tribocharging, although this not considered here as such effects are typically encountered with dissimilar materials (Matsusaka et al. 2010). The morphology of particles also plays a key role regarding the bulk behavior of a powder as irregularly shaped particles, often generated by satellisation and agglomeration of otherwise spherical particles during the atomization process, may become entangled by mechanical interlocking. Satellited particles and agglomerates can for instance be observed by Scanning Electron Microscopy (SEM) imaging of an Aluminium-Copper (casting alloy 224.0) powder, as shown in figure 1, where lot A displayed on the left

contains many agglomerates and satellites compared to lot B, which was atomized in different conditions (shape of the atomization nozzle, oxygen content etc.) and presents fewer satellites and agglomerates.

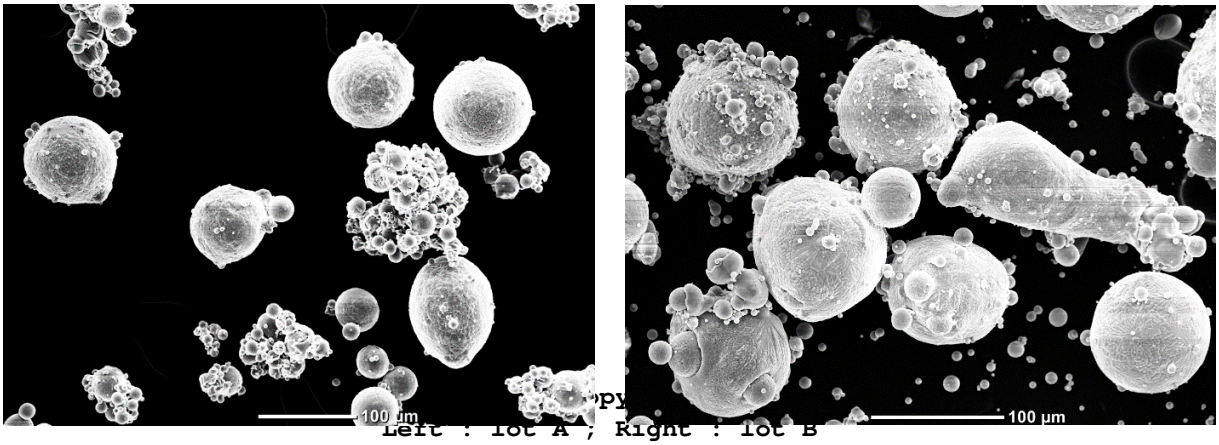

Left : lot A ; Right : lot B

The granular Bond number, defined as the ratio of adhesion forces F_a applied on a particle to its weight W as shown in equation 1, is a well-known criterion for estimating the flowability of a monodisperse distribution of particles (Castellanos 2005).

$$Bo_g = F_a/W \qquad (1)$$

However, the size of metal AM powder particles produced by gas atomization typically varies according to a log-normal distribution (see figure 2) which is parameterized by a mean μ and a standard deviation σ according to equation 2, which is not included in equation

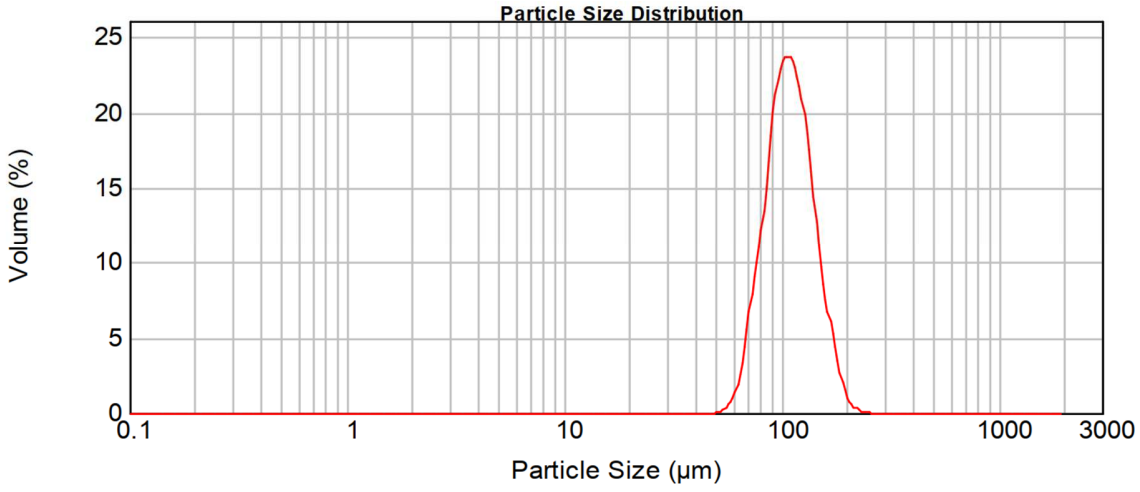

1.

Figure 2 : Log-normal distribution of a 224.0 Al-Cu gas atomized powder

$$f(x|\mu,\sigma) = \frac{1}{x\sigma\sqrt{2\pi}}\exp\left(-\frac{(\ln(x)-\mu)^2}{2\sigma^2}\right) \quad (2)$$

The mean and standard deviation can be approximated using commonly reported D-values such as d_{10}, d_{50} and d_{90}, as shown in equations 3 and 4.

$$\mu = \ln(d_{50}) \quad (3)$$

$$\sigma = \ln\left(\frac{d_{50}}{d_{16}}\right) = \ln\left(\frac{d_{84}}{d_{50}}\right) \approx \ln\left(\frac{d_{90}}{d_{50}}\right) \approx \ln\left(\frac{d_{50}}{d_{10}}\right) \quad (4)$$

To account for particle size disparity, a population-dependent granular Bond number (equation 5) is calculated based on a weighted average over the size distribution of the granular Bond number between particles (Capece et al. 2015, 2016). The particle size distribution is approximated as multiple discrete bins of constant particle size, and the average granular Bond number within and between bins is calculated through equation 6. A weighted sum based on a weight coefficient $w_{k,l}$, computed based on the fractional surface area of each bin of particles with respect to the total surface area, yields an average of the granular Bond number over the particle size distribution.

$$Bo_g^* = \left(\sum_{k=1}^{L}\sum_{l=1}^{L}\frac{w_{kl}}{Bo_{g,kl}}\right)^{-1} \quad (5)$$

$$Bo_{g,kl} = \frac{F_{a,kl}}{W_{kl}} \quad (6)$$

This population-dependent granular Bond number Bo_g^* has been successfully applied to pharmaceutical powders as it showed a good correlation with a typical flowability measurement method based on a flow function coefficient obtained by shear cell measurements (Capece et al. 2016). The Bo_g^* criterion is here applied to metal AM powders as the basic principles remain applicable to both organic and metallic

materials. The advantage of a flowability criterion such as Bo_g^* is that it is directly based on physical models of interaction forces and explicitly accounts for particle polydispersity. It can therefore provide a theoretical assessment of powder flowability and help quantify the relative importance of various known properties such as particle density, median diameter etc.

b. Interaction forces

The adhesion force model originally used for calculating Bo_g^* originally only includes a simplified model of van der Waals forces (Capece et al. 2016; Chen et al. 2008). In this paper, both van der Waals and capillary force models are included in the Bo_g^* criterion formulation, with the use of more recent force based on a 2-scale roughness model (double immersed spheres) that is more apt in capturing the effect of surface asperities on the magnitude of the adhesion forces between particles (LaMarche et al. 2016, 2017; Liu et al. 2016). To account for differences in particle sizes between bins when calculating adhesion and gravitational forces, geometric or arithmetic means are used where needed, similarly to (LaMarche et al. 2017). For instance, the capillary force model (LaMarche et al. 2016) only accounts for particles with the same diameter, so an equivalent diameter is computed based on an arithmetic mean of particle radii. The more recent van der Waals force model employed here for calculating Bo_g^* and given by equation 7, already accounts for differences in particle sizes. This equation is essentially a sum of van der Waals force contributions resulting from the interaction between spheres of various scales that represent the particles and their surface roughness. The geometry of the double-immersed spheres can be directly derived from root mean square and wavelength measurements on 2 scales of surface roughness.

Another important parameter for calculating van der Waals forces is the Hamaker constant. A review of Hamaker values found in the literature for materials of interest are displayed in table 1. It can be noted that the values of Hamaker constants for metals and oxide are less commonly reported than for inorganic materials, and there is some discrepancy between the values given by the various studies.

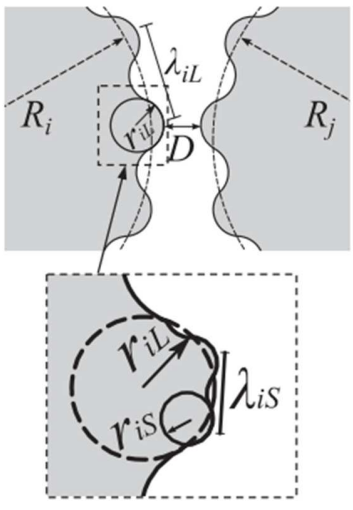

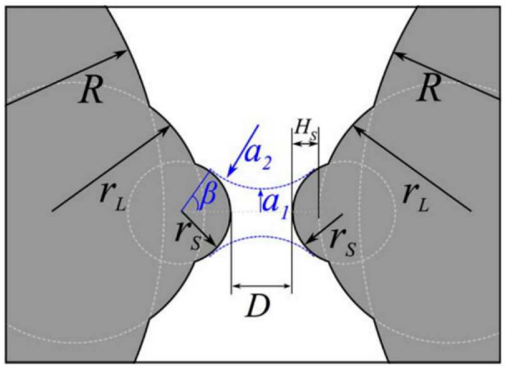

Figure 3 : Left – Roughness model for van der Waals force calculation (LaMarche et al. 2017; Liu et al. 2016) ; Right – Roughness model for capillary force calculation (LaMarche et al. 2016)

$$F_{vdW_{ij}} = \frac{A_{ij}}{6}\left[\frac{R_iR_j}{(R_i+R_j)\left(D+y_{iL}+y_{iS}+y_{jL}+y_{jS}\right)^2} + \frac{R_ir_{jL}}{(R_i+r_{jL})\left(D+y_{iL}+y_{iS}+y_{jS}\right)^2} + \right.$$
$$\frac{R_ir_{jS}}{(R_i+r_{jS})(D+y_{iL}+y_{iS})^2} + \frac{r_{iL}R_j}{(r_{iL}+R_j)\left(D+y_{jL}+y_{jS}+y_{iS}\right)^2} + \frac{r_{iS}R_j}{(r_{iS}+R_j)\left(D+y_{jS}+y_{jL}\right)^2} + \quad (7)$$
$$\left.\frac{r_{iL}r_{jL}}{(r_{iL}+r_{jL})\left(D+y_{iS}+y_{jS}\right)^2} + \frac{r_{iL}r_{jS}}{(r_{iL}+r_{jS})(D+y_{iS})^2} + \frac{r_{iS}r_{jL}}{(r_{iS}+r_{jL})\left(D+y_{jS}\right)^2} + \frac{r_{iS}r_{jS}}{(r_{iS}+r_{jS})D^2}\right]$$

$$k_1 = 1.817,\ r_{kl} = \frac{\lambda_{kl}^2}{32k_1rms_{kl}},\ y_{kl} = k_1rms_{kl}\ \ with\ k = i,j\ and\ l = S,L$$

Material (media 1)	$\boldsymbol{A_{131}(=A_{11})}$ (media 3 : inert air or vacuum) x10^{-20} J	$\boldsymbol{A_{131}}$ (media 3 : water) x10^{-20} J
α–Al_2O_3	15.2[a] ; 16[b]	3.67[a] ; 5.3[b]
TiO_2	15.3[a]	5.35[a]
Al	33[d] ; 25.6[e]	18.4[e]
Fe	26[d]	10.08[h]
Cu	28.4[d'] ; 40[c,d'] ; 46[d] ; 27.8[e] ; 24.82[e] ; 27.20[e']	14.4[e] ; 11[f]
Metals (Au, Ag, Pt...)	~40[c]	19.4[h]
PTFE	3.63[e]	0.33
H_2O	3.7[c]	–

Table 1 : Nonretarded Hamaker coefficients

a: based on the full Lifschitz theory (Bergström 1997)
b: (Götzinger and Peukert 2003)
c: reported in (Israelachvili 2011)
d: calculation from (Osborne-Lee 1988)
d': reported in (Osborne-Lee 1988)
e: calculation from (Jiang and Pinchuk 2016)
f: calculation from (Lefèvre and Jolivet 2009)
g: calculation from (Leite et al. 2012)

g' : experimental value from (Leite et al. 2012)
h: estimated using a combining rule

The capillary force model is based on (LaMarche et al. 2016), which relies on a classic sum of contributions of surface tension of the capillary bridge and pressure difference Δp_l, as shown in equation 8. The pressure difference Δp_l can be evaluated based on the Kelvin equation (equation 9) and the Laplace–Young equation (equation 10). Further details on the iterative process required for solving these equations, including coefficients a_1 and a_2 and angle β (see figure 3), can be found in (LaMarche et al. 2016).

$$F_{cap} = 2\pi a_1 \sigma_{cap} + \pi {a_1}^2 \Delta p_l \quad (8)$$

$$\Delta p_l = -\bar{\rho}_l R_g T \, ln(RH) \quad (9)$$

$$\Delta p_l = -\sigma_{cap}\left(\frac{1}{a_2} + \frac{1}{a_1}\right) \quad (10)$$

Advantageously and unlike prior roughness models, the 2-scale roughness model can be directly linked to roughness measurements (LaMarche et al. 2017). However, despite the importance of surface roughness in calculating adhesion forces, almost no information is available on the surface roughness of the gas atomized metal AM powder particles of the present study, and little information is generally available in the literature. Values on the order of 1 to 10nm found in the literature presented in table 2 are used here (Laitinen et al. 2013). These measurements are most likely a lower bound on particle roughness as they concern surface remelted alumina particles, and are advantageously formulated as a 2-scale roughness, as in the van der Waals and capillary force models. In the literature, a much larger value of 200nm is widely quoted as a natural roughness for organic or pharmaceutical particles (Capece et al. 2014; Castellanos 2005; Huang et al. 2015). The actual roughness of metal AM particles must then lie somewhere in-between those orders of magnitude, i.e. around 10 to 100nm, however there is little data available in the literature regarding gas atomized metal particles. The roughness is thus considered to be identical for all Bo_g^* calculations.

Material	rms_S	rms_L	λ_S	λ_L
Alumina	1.5–12nm	12nm	0.7µm	10.2µm

Table 2 : Roughness values used for van der Waals and capillary force models (Laitinen et al. 2013)

Considering the lack of published data or direct measurements associated with some parameters such as particle roughness and Hamaker constants, flowability criterion Bo_g^* is here evaluated in relative terms by normalizing it by the $Bo_{g,ref}^*$ value calculated for a reference powder, i.e. $Bo_{g,rel}^* = Bo_g^*/Bo_{g,ref}^*$.

Some rough calculations of $Bo_{g,rel}^*$, obtained through a MATLAB code, are given in table 3 to illustrate the role of some powder characteristics on flowability. Everything else remaining equal, an increase in median diameter, a decrease in span, an increase in density or a decrease in relative humidity induce a flowability improvement. Although this could be intuitively expected, criterion $Bo_{g,rel}^*$ demonstrates it explicitly based on physical models, and helps quantify the sensitivity to each parameter. For instance, it appears from table 3 that doubling the median diameter is much more effective for improving flowability than halving the span.

Material	**Density (g/cm³)**	**Hamaker constant (zJ)**	d_{50} **(µm)**	**span**	**%RH**	$Bo_{g,rel}^*$
224.0	2.841	293	65	0.69	41	1
316L	8.0	293	65	0.69	41	0.34
224.0	2.841	146.5	65	0.69	41	0.70
224.0	2.841	586	65	0.69	41	1.50
224.0	2.841	293	65	0.69	20.5	0.78
224.0	2.841	293	65	0.69	82	2.48
224.0	2.841	293	130	0.69	41	0.12
224.0	2.841	293	32.5	0.69	41	7.79
224.0	2.841	293	65	0.345	41	0.90
224.0	2.841	293	65	1.38	41	1.57

Table 3 : Variations of flowability criterion $Bo_{g,rel}^*$

In summary, this section suggests an improvement on an existing flowability criterion by including a 2-scale roughness van der Waals force model and a capillary force model, as well as a normalization of the flowability criterion with respect to a reference powder with passable flowability to recover the usual unity threshold of flowability criteria. Some preliminary calculations offer an evaluation of the sensitivity of this flowability criterion with respect to various powder characteristics, including its size distribution and humidity levels. To estimate the appropriate parameters for the 2-scale roughness van der Waals force model, a

literature review of Hamaker constants of various materials of interest is given, highlighting the variability and lack of reliable data for most metals. Similarly, some roughness values found in the literature are also provided, which again shows the scarcity of such measurements for gas atomized AM powders.

3. Flowability enhancement by vibrational assistance

a. Identification of vibrational frequency for flowability enhancement

Some aluminium-based AM powders present a high degree of cohesiveness due to their low density, high span, and presence of satellites. These powders do not flow adequately through funnel flowmeters so that their relative flowability cannot be compared with these methods, in spite of the fact that these funnel-based flowability measurement methods are among the most suitable for assessing in-process flowability as the powders are in a similar state of compaction as in an LMD reservoir. Other common flowability measurement methods include ring shear cell testers, where the powder is highly compacted and thus does not properly reflect the compaction state of powders inside an LMD reservoir. Optical evaluation can also be used but it does not provide an absolute quantification of flowability measurement as it typically relies on a relative ranking of flowability based on a visual evaluation by a human operator. Avalanche angles formed by a powder at rest is another flowability measurement method that requires the powder to flow through a funnel in the first place, and is not repeatable for highly cohesive powders (Spierings et al. 2015). To circumvent this issue and thus enable a funnel-based flowability assessment of cohesive powders, a vibrational assistance is provided to the sidewalls of a funnel.

The use of vibrations to enable or control the flow of powders has previously been reported in a number of studies, as reviewed in (Yang and Evans 2007), and has for example been applied to micro-dosing of polymer powders for powder bed process (Stichel et al. 2014, 2016) and organic powders (Dunst et al. 2018) as vibrations could alleviate the effect of friction forces and thereby increase the flowability. Conversely, it has also been reported that vibrations could lead to compaction of pharmaceutical powders and thus diminish their flowability (Polizzi et al. 2016). The impact of vibrations is thus generally unclear as the effect on flowability depends on many factors such as powder composition, morphology, and vibration mode (Stichel et al. 2016). There are currently no known published studies on the

impact of vibrations on the flowability of gas atomized metal AM powders. Moreover, previous studies generally focused on low-frequencies (i.e. < 1kHz) or ultrasonic regime (i.e. > 20kHz), although, as it turns out, the flowability improvement for metal AM powders shown thereafter occurs in the range 1kHz-10kHz with the current experimental setup. Additionally, it is noted that appropriate vibrational assistance can not only enable the control of non-free-flowing powders, as demonstrated in other studies, but can also be employed as a flowability characterization method for highly cohesive powders, as will be shown in this section.

The experimental setup developed in the laboratory uses a non-standard funnel with the same taper angle as Hall and Carney flowmeters (i.e. 60°) but a slightly larger opening (i.e. 6mm). This funnel is made of a light polymer material that facilitates the transmission of the vibrations towards the powder bulk. A piezoelectric transducer is attached to the sidewall of the funnel and is linked to a function generator that provides a sine signal at 10Vpp. The frequency of the signal is varied between 1 and 10kHz and the funnel flowability of two aluminium-copper powders, described in table 4, is measured and displayed in figures 4 and 5. The measurement is not expressed in s/50g as usually done in the literature but rather in cm3/s, i.e. an average volumetric flowrate, to avoid infinite values for no-flow conditions.

A sharp increase in flowability is identified in both cases around 3kHz. As the frequency reaches the end point of the frequency range, i.e. 1 and 10kHz, the flowability falls back down to 0 as obtained without any vibrational assistance. Going beyond this range in the positive (i.e. up to 100kHz) and negative direction (i.e. down to 1Hz) did not uncover any other favorable regime. The flowability improvement near the resonant frequency can be linked to a decrease in friction forces (Dunst et al. 2018) and adhesion forces due to a local displacement of individual particles. This in turn favors the breakage of particle force chains, thereby destabilizing the structure formed by the cohesive, non-free-flowing particle inside the hopper. As the result, the flow of cohesive powders is not only triggered but is also sustained by the continuous application of vibrations on the sidewall.

Powder	**Composition**	**Sieve Granulometry (approx.)**
224.0-A	Al-Cu4.7-Mn-Ti-V-Zr	63-80µm
AM205	Al-Cu5-Ti-B-Ag-Mg-Si	20-63µm

Table 4 : Powders used for resonant frequency identification

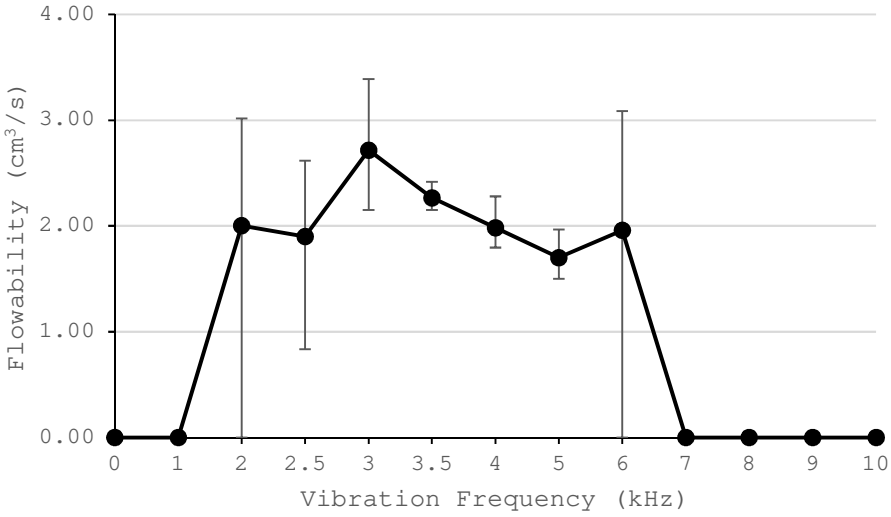

Figure 4 : Flowability vs. Vibration frequency for 224.0-A cohesive Al-Cu AM powder

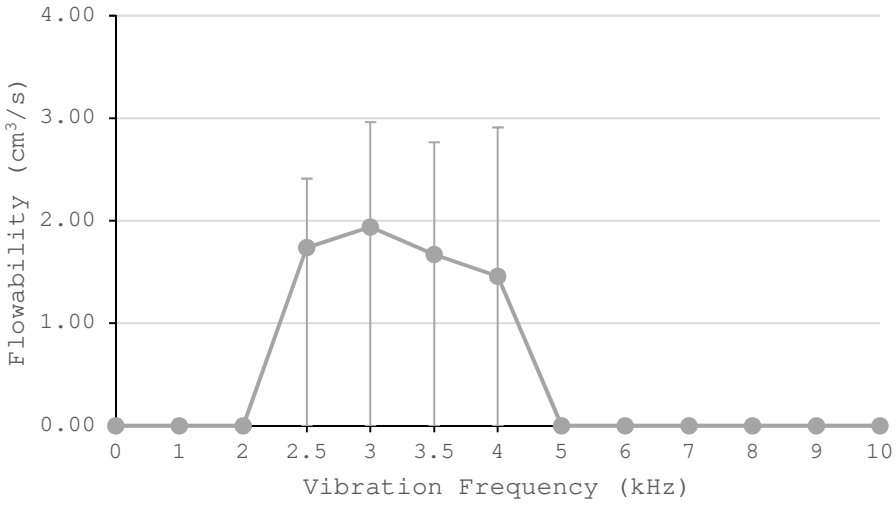

Figure 5 : Flowability vs. Vibration frequency for AM205 cohesive Al-Cu AM powder

Given the measurements presented in figures 4 and 5, a resonant frequency can be identified near 3kHz for the considered aluminium powders. This resonant frequency identified through forced continuous horizontal vibrations should typically correspond to the natural frequency of the powder-funnel system, so that the amplitude of individual particle motion is amplified around this frequency of external excitation, to the point where it breaks the force chains or "bridges" between the particles and the funnel walls that prevented

powder flow. This leads to a collapse of the particle chain structure and triggers an avalanche of particles down the funnel. The natural frequency of the system notably depends on powder properties (material, size distribution) as well as funnel geometry, and is thus difficult to predict analytically. When the forced excitation is applied at a frequency far from the natural frequency of the system, the amplitude of particle motion is largely dampened throughout the particle bulk, and can also yield an adversarial effect of increased packing efficiency that further strengthens the force chain structure and thereby increasingly prevents funnel flow (Polizzi et al. 2016; Yang and Evans 2005).

All subsequent flowability measurements with vibrations will thus employ this frequency. Although some variation on the exact resonant frequency can be expected across various powder composition and granulometry, a single constant value is used here as a first approximation.

b. Application of vibration assistance at resonant frequency

In table 5, 15 powder samples are listed along with their general chemical composition, median diameter, span, as well as the corresponding flowability measurements through the non-standard funnel used in the experimental setup, with and without vibrations being applied through the piezoelectric transducer. For each flowability measurement, a volume of 25cm^3 (+/- 0.5) is placed inside the flowmeter and the vibratory signal at 3kHz with a sine waveform is started. The outlet of the hopper is then opened and the flowing time of the sample is measured. Each measurement is performed 5 times. The $Bo^*_{g,rel}$ criterion is normalized with respect to reference powder Al12Si-B where it is set to unity. The average results shown in green color in table 5 correspond to cases where the experimental flowability measurements or $Bo^*_{g,rel}$ calculations are significantly better than the results of the reference powder considering the standard deviation shown in parenthesis. Conversely, results in red are significantly worse, and uncolored results are not significantly different, usually due to a relatively large standard deviation. The largest discrepancy between measurements and $Bo^*_{g,rel}$ calculations occurs with powder Al7Si6Mg. This may be caused by unaccounted for mechanisms such as increased mechanical interlocking due to non-sphericity of particles, or by the insufficient weight of powder distribution span in the $Bo^*_{g,rel}$ criterion

formulation, as suggested by the statistical analysis thereafter where the span and specific volume are also significant factors.

The $Bo^*_{g,rel}$ calculation result, evaluated through a MATLAB code, is also given in table 5 based on powder characteristics (granulometry, density, Hamaker constant), environmental conditions (temperature and relative humidity) and other parameters that are assumed to be constant and identical for a lack of better data (e.g. Hamaker constant, equilibrium separation distance between particles, surface roughness). Note that the Bo^*_g does not account for the presence of vibrations, friction forces and mechanical interlocking forces.

Powder	d_{50}	Span	Flowability (no vibrations) [cm³/s]	Flowability (with vibrations) [cm³/s]	$Bo^*_{g,rel}$
224.0-A 20-80µm	39.2	1.37	0,00 (0)	0,36 (0.26)	4.27
224.0-A 45-90µm	60.6	0.74	0,00 (0)	2,91 (0.25)	1.12
224.0-A 63-80µm	70*	0.43*	0,00 (0)	2,75 (0.39)	0.74
224.0-A 80-100µm	101.0	0.77	3,49 (0.73)	3,90 (0.69)	0.24
224.0-A 100-125µm	120.0	0.78	3,14 (0.22)	2,93 (0.37)	0.14
224.0-B 90-125µm	108.9	0.65	4,58 (0.05)	5,51 (0.69)	0.19
224.0-B 125-150µm	143.3	0.64	5,38 (0.13)	5,47 (0.20)	0.08
224.0-B 150-250µm	203.3	0.66	6,06 (0.33)	6,45 (0.08)	0.03
AM205 20-63µm	39.16	0.86	0,00 (0)	1,94 (1.07)	5.4
Al7Si6Mg 30-150µm	78.6	1.40	0,00 (0)	2,11 (0.09)	0.90
Al12Si-A 45-90µm	62.4	0.67	3,27 (0.42)	4,14 (0.51)	1.08
Al12Si-B 45-90µm	65*	0.69*	2,71 (0.03)	2,70 (0.01)	1.0
316L 45-90µm	65*	0.69*	5,63 (1.53)	6,28 (0.09)	0.31
Fe38MnSiV 45-90µm	67.2	0.71	6,81 (0.22)	6,65 (0.14)	0.28
Ti6Al4V 45-90µm	64.0	0.53	5,66 (0.31)	6,39 (1.68)	0.31

Table 5 : Powder characteristics and average (std. dev.) of flowability measurements (with and without vibrations at 3kHz) of 15 metal AM powder samples, with sample Al12Si-B used as a reference (green : satisfactory flowability – red : unsatisfactory flowability)

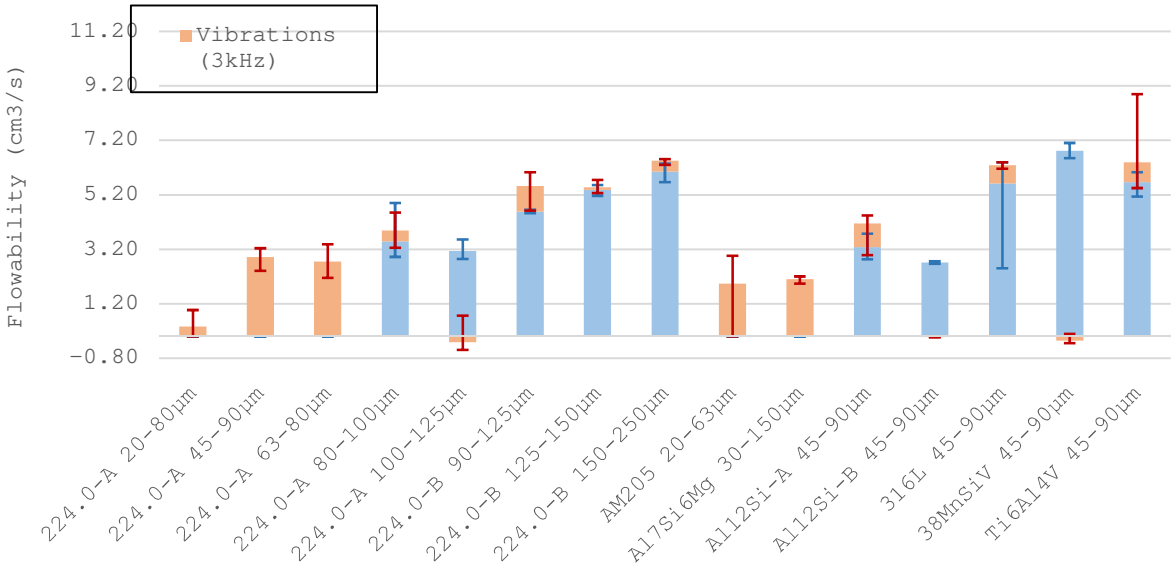

Figure 6 : Flowability with and without vibrations at 3kHz of 15 metal AM powder samples

Figure 6 summarizes the results presented in table 5. The green color in the table represents samples with better experimental or theoretical flowability than reference powder Al12Si-B, whereas conversely the red color indicates that the sample flowability is inferior. When subjected to 3kHz vibrations, the most cohesive powders (224.0-A 20-80µm, 224.0-A 45-90µm, 224.0-A 63-80µm, AM205 20-63µm, Al7Si6Mg 30-150µm), which do not flow through the hopper without vibrations, undergo a significant improvement in flowability, whereas the least cohesive powders (224.0-B 125-150 µm, 316L 45-90µm, 38MnSiV 45-90µm, Ti6Al4V 45-90µm) are subject to a more modest or even insignificant variation in flowability. Among moderately cohesive powder samples (224.0-A 80-100µm, 224.0-A 100-125µm, Al12Si-A 45-90µm, Al12Si-B 45-90µm), sample Al12Si-A 45-90µm presents a notable increase in flowability with the addition of vibrations, whereas the flowability change with the other aforementioned samples is much less significant. It can also be noted that powder samples from the same batch, i.e. the same chemical composition, undergo an increase in flowability with an increase in median diameter and a decrease in span.

Generally, the most cohesive powders form a stable bridge inside the flowmeter or flow in a rat hole or funnel flow regime, whereas the least cohesive powders flow in a funnel flow to mass flow regime (Carson and Pittenger 1998). In a mass flow regime, particles flow at the same velocity while in a funnel flow regime, particles flow faster in the center of the hopper. The powders flowing in a mass flow regime, such as 316L and Ti6Al4V, already flow near the maximum possible rate given the taper angle and aperture diameter of the flowmeter, so that vibrations have an insignificant effect in such cases. In contrast, powders that flow irregularly in a rat hole regime or in a funnel regime, have room for improvement in terms of average mass flowrate, which explains the greater impact of vibrational assistance in such cases as it diminishes interparticle forces. For powders that do not flow at all without vibrations, the arc bridges formed by particle force chains between the sidewalls of the flowmeter can be destabilized by the local displacement of particles induced by the application of vibrations at an adequate frequency and amplitude, so that the vibrational assistance can trigger and sustain the flow of an otherwise non-flowing powder. In summary, the more cohesive the powder, the greater is the potential for vibration-based flowability improvement.

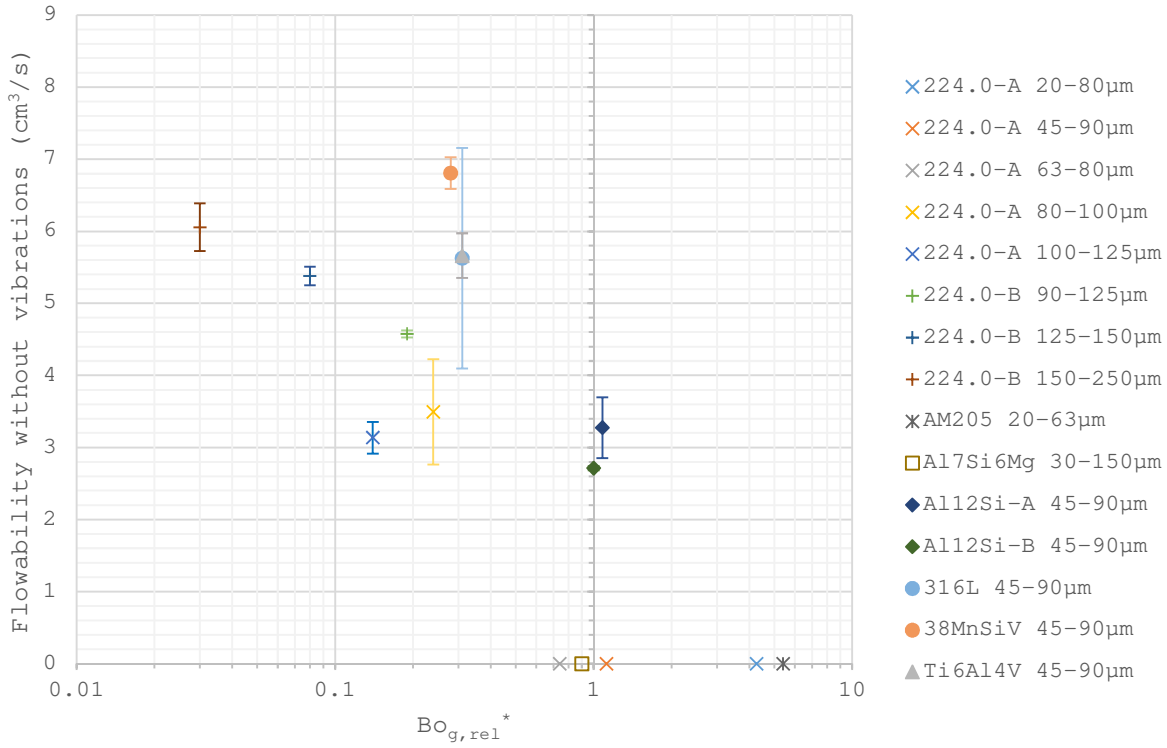

Figure 7 : Flowability without vibrations versus Flowability criterion $Bo^*_{g,rel}$

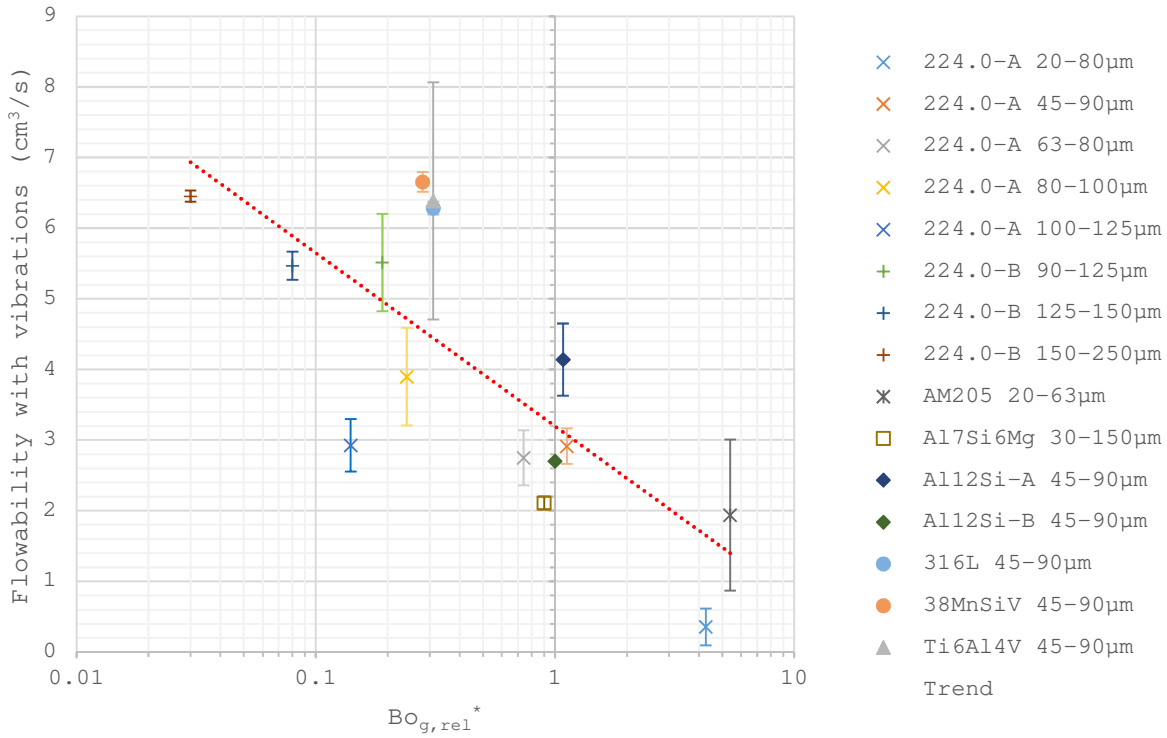

Figure 8 : Flowability with vibrations at 3kHz versus Flowability criterion $Bo^*_{g,rel}$

Figures 7 and 8 illustrate the relation between flowability measurements without vibrations and $Bo^*_{g,rel}$ and the relation between flowability measurements with vibrations and $Bo^*_{g,rel}$, respectively. The most drastic change in flowability between those figures occurs for the most cohesive powders, i.e. the powders with the smallest flowability and generally the highest $Bo^*_{g,rel}$ values. In figure 8 where vibrations are applied, a quasi linear relationship illustrated by the dotted red line appears between $\ln(Bo^*_{g,rel})$ and flowability measurements. An ANOVA analysis of the results of figure 8 is shown in table 6, which reveals that the logarithm of flowability criterion $Bo^*_{g,rel}$ along with span and specific volume (or almost equivalently density) and their higher order combinations can together explain 95% of the variability in flowability between powder samples, without the regression model overfitting the data (i.e. $R^2_{adj} = 0.953$ is close to $R^2_{pred} = 0.949$ and p-values are small compared to the typical threshold of 0.05).

	Sum of Squares	dof	F-value	p-value
Model	328,85	11	196,46	< 0.0001
C- $\ln(Bo^*_{g,rel})$	41,33	1	271,62	< 0.0001
E-span	39,70	1	260,86	< 0.0001
H-specific volume	40,40	1	265,50	< 0.0001
CE	39,69	1	260,85	< 0.0001
CH	40,75	1	267,79	< 0.0001
EH	40,06	1	263,25	< 0.0001
C²	43,70	1	287,17	< 0.0001
H²	38,01	1	249,78	< 0.0001
CEH	39,80	1	261,57	< 0.0001
C²H	43,61	1	286,56	< 0.0001
CH²	41,40	1	272,05	< 0.0001
Residual	14,46	95		
Lack of Fit	2,31	3	5,82	0,0011
Pure Error	12,15	92		
Total	343,31	106		

Table 6 : ANOVA results for flowability experiments with vibrations at 3kHz

This suggests that vibrations help alleviate the effect of forces that were unaccounted for such as friction and mechanical interlocking. Indeed, the presence of vibrations near the resonant frequency diminishes the impact friction forces (Dunst et al. 2018) and mechanical interlocking forces through local displacements of particles within the powder bulk. This explains the fact that most of the variability in flowability is accounted for when vibrations are applied despite the fact that those potentially important contributions are ignored.

There is also a lack of accurate data regarding surface roughness and Hamaker constant for the metal powders under study. It is expected that including refining the values of these parameters in the $Bo^*_{g,rel}$ calculations would provide a more complete view of the flowability variation between powder samples and improve the predictability of criterion $Bo^*_{g,rel}$, notably in the case where vibrations are not applied. However, as a first approximation, this criterion already yields satisfactory results using only commonly available parameters such as D-values and particle density.

While not shown here, it is also noted that the amplitude of the vibratory signal not only can trigger and sustain powder flow but may also help control the flowrate of powder, as found in previous work regarding vibrational assistance (Yang and Evans 2007).

In summary, this section showed that a vibrational assistance provided continuously to a funnel flowmeter at a proper frequency could help trigger and sustain the flow of cohesive metal AM powders. Based on a statistical analysis of the flowability measurements with vibrations and crude calculations of the $Bo^*_{g,rel}$ criterion with the available data on powder characteristics, it appears that this flowability criterion together with the span and specific volume are significant in explaining the observed variations of flowability with vibrations between powder samples. This suggests that this flowability criterion could be used as an indicator of powder flowability that can be calculated based on typical powder characteristics, including its particle size distribution.

The adequacy between flowability measurements and this indicator could be further improved by the knowledge of particle roughness as well as including the effects of non-sphericity and other cohesive forces such as friction and mechanical interlocking, which are however non-trivial to assess with a purely analytical model. However, this would allow $Bo^*_{g,rel}$ to better evaluate powder flowability without vibrations. Indeed, the use of vibrational assistance most likely counterbalances those ignored effects and thus helps explain the superior predictability of $Bo^*_{g,rel}$ for flowability measurements with vibrations compared to flowability measurements without vibrations. It is also noted that the

span and specific volume are also significant factors in explaining powder flowability with vibrations despite their inclusion in the $Bo^*_{g,rel}$ formulation, so that an improved formulation of $Bo^*_{g,rel}$ may be required to better include these aspects and thereby enable the use of a single analytical criterion to predict powder flowability.

4. Flowability enhancement by heat treatment

Gas atomized powders based on a 224.0 casting alloy ingot present a poor flowability as is. Vibrational assistance is not usually available in the LMD distribution system, and sieving operations to increase the median diameter and diminish the span of the particle size distribution is not sufficient to obtain a satisfactory in-process flowability. Another approach for improving the flowability of metal AM powders is presented here, which relies on a specific heat treatment defined by a time-temperature profile under a dry air atmosphere.

Generally, the time-temperature setting for drying and preheating metal AM powders is typically on the order of 2h at 80°C to 120°C according to technical documentation provided by suppliers. However, these time-temperature values do not yield a significant in-process flowability improvement.

Gradually increasing the time and temperature settings from 2h at 80°C to 10h at 180°C reveals that a heat treatment of cohesive Al-Cu powders at 180°C for 10 hours induced a significant improvement in flowability, both in the flowmeter and in-process at the LMD reservoir. The in- flowability is not directly quantifiable so that the flowmeter-based flowability measurements are given in table 7, with and without vibrational assistance. The mechanism for flowability improvement is two-fold.

Firstly, the drying effect caused by the increased time and temperature allows to remove the residual humidity adsorbed on the porous alumina layer that is formed spontaneously at the aluminium particle surface upon contact with oxygen in the atmosphere (Götzinger and Peukert 2003). In table 7, the average relative humidity within the powder sample is much lower after the heat treatment, which is reflected in the decrease in $Bo^*_{g,rel}$ values due to the weaker capillary force magnitude that results.

The time-temperature setting of 180°C for 10h is akin to artificially aging or precipitation hardening of casting alloy 224.0 that can promote the formation of Al_2Cu phases and thereby strengthen the

material (CIRAL et al. 1996; Dumant 1996; Planchamp et al. 1993). Precipitation hardened materials typically undergo an improvement in strength, and notably in terms of yield strength. While Young's modulus is generally barely unaffected by changes in microstructure, it can vary under a phase change such as when copper dissolved in the aluminium matrix precipitates into the hard and brittle phase Al_2Cu. This means that individual particles are less deformable under the weight of other particles located on top, so that the contact surface between particles is reduced. As a result, contact forces such a sliding and rolling friction as well as adhesion forces such as van der Waals forces are also diminished, which in turn improves the flowability of the powder. It is noted that the $Bo^*_{g,rel}$ criterion as presented in this work does not explicitly include this hardening effect as it only considers rigid particles in its force models of van der Waals and capillary forces and ignores friction forces.

Another possible mechanism for flowability enhancement could reside in the increase in oxidation levels on the surface of the particles in the form of alumina. Because alumina is a hard and brittle material, it could contribute to an increase in overall rigidity of the particles, similarly to the precipitation hardening effect, by reducing the deformability of the particles and thus improve their flowability. However, the alumina layer formation is self-limiting so that it typically barely exceeds 5nm in thickness in dry air conditions (Hatch 1984). This surface hardening effect is likely to be insignificant compared to the precipitation hardening of the bulk of the particles. Alumina layer thickness measurements would be needed to precisely assess this effect, however such measurements are challenging to conduct considering the very small thickness of the oxidation layer and are thus beyond the scope of the present work.

Powder	***T*** **(K)**	***RH*** **(%)**	**Flowability (no vibrations) [cm³/s]**	**Flowability (with vibrations) [cm³/s]**	$\mathbf{Bo^*_{g,rel}}$
224.0-A 63-80µm	25.7	40.5	0 (0)	2,75 (0.39)	0.74
Dried 224.0-A 63-80µm	80-30	8-18	3.16 (1.18)	4.10 (1.75)	0.54
224.0-B 90-125µm	25.8	41.7	4,58 (0.05)	5,51 (0.69)	0.19
Dried 224.0-B	80-40	8-17	5.06 (0.03)	6.11 (0.09)	0.14

90-125µm	

Table 7 : Flowability variation with temperature and humidity

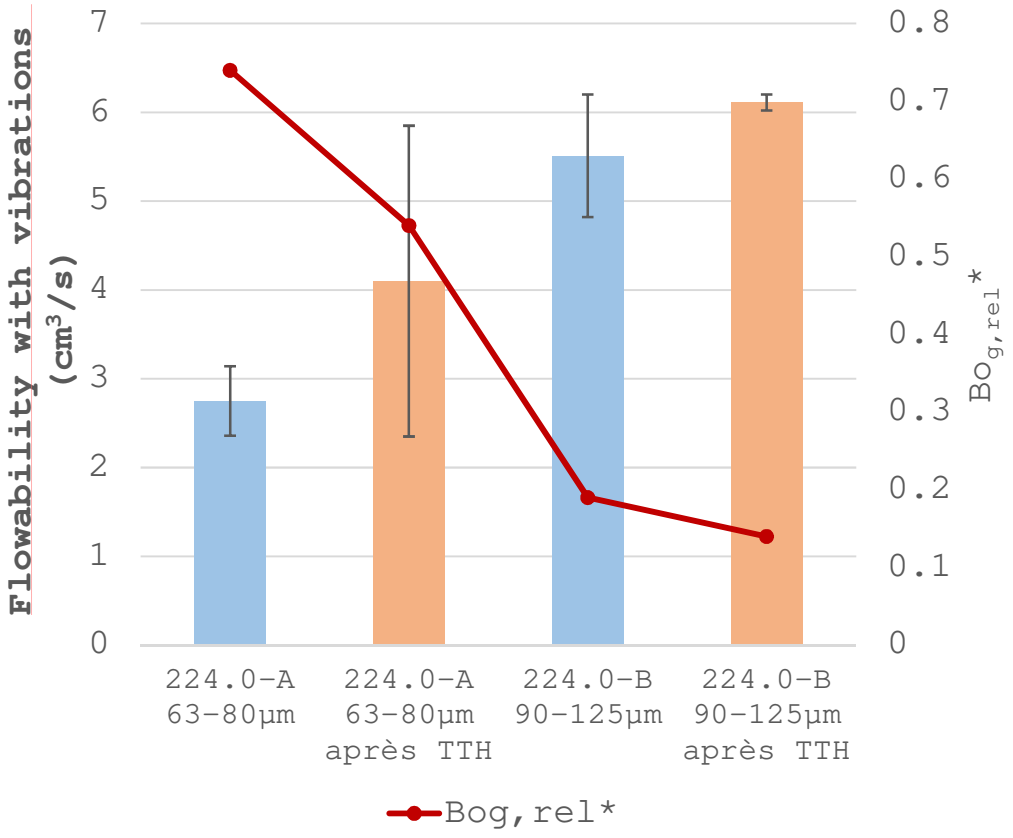

Figure 9 : Flowability measurement and $Bo^*_{g,rel}$ values before and after heat treatment for powders 224.0-A 63-80µm and 224.0-B 90-125µm

5. LMD processing of cohesive aluminium-copper powders

The heat treatment applied on cohesive powders 224.0-A 63-80µm enabled the in-process use of these powders in the context of LMD, for example to build single track walls with various process parameters as illustrated on figure 10. In contrast, the untreated powder could not be made to flow down the powder reservoir despite a fairly small span and a relatively high median diameter compared to typical commercial LMD powders with a sieve range of 45-90µm.

Figure 10 : Fabrication of single-track walls with powder 224.0 enabled after flowability improvement through heat treatment

An increase in median diameter, as well as a decrease in span and humidity contents lead to an improvement in flowability for metal AM powders. These tendencies were highlighted in a recent review (Vock et al. 2019) and were supported by $Bo^*_{g,rel}$ calculations in table 3. It also appears that the heat treatment provides another flowability improvement mechanism beyond a drying effect since the usual time-temperature settings for powder drying did not yield a satisfactory in-process flowability. It can be hypothesized that increasing the time-temperature setting provides an increase in particle hardness due to precipitation hardening, which is consistent with the usual heat treatment settings applied after casting such alloys (CIRAL et al. 1996; Planchamp et al. 1993). This increase in hardness leads to less deformable particles that are less affected by adhesion and friction forces due to a diminished contact surface area between neighbor particles, and thus flow more easily inside the LMD distribution system. The significant improvement in flowability enabled the use of these Al-Cu powders to exit the distribution system in a homogeneous and regular manner, allowing their pneumatic transport towards the LMD nozzle and ultimately their fusion/solidification by the laser.

Conclusion

In the theoretical section of this work, it was showed that a flowability criterion, the relative population-dependent granular Bond number $Bo^*_{g,rel}$, can help characterize powder flowability based on commonly reported powder characteristics (material density, D-values etc.) and improved interaction force models. Although it was here applied to log-normally distributed metal AM powders, it is general in nature and could be applied to many other types of particle size distributions. In this work, more recent force models were included in the calculation of this criterion compared to the literature. A capillary force model was combined to a van der Waals force models that both make use of a 2-scale roughness geometry model that is not only more representative of actual surface roughness but can also be directly linked to roughness measurements. This flowability criterion could be further improved by obtaining accurate roughness data for each powder sample, for instance through Atomic Force Microscopy measurements, as well as more precise values of Hamaker constants, which are currently lacking in the literature as shown in section 2 of this paper. Moreover, other forces such as sliding and rolling friction, mechanical interlocking forces related to particle morphology could also be added, as well as particle deformation to account for hardening effect. However, no straightforward analytical models exist to account for these effects.

Additionally, one of the main experimental findings of this paper is that the use of vibrations at a specific frequency, i.e. near 3kHz in the current setup, can significantly improve the flowability of metal AM powders, especially cohesive aluminium powders. Not only does this provide a fairly simple setup evaluate the flowability of metal AM powder (both free-flowing and non-free-flowing) in a repeatable manner, it also hints at the use of vibrational assistance inside the LMD system at an adequate frequency to enhance the flow of powder in strategic locations throughout the distribution system. Further experiments could refine the variation in flowability with the variation in signal frequency for non-aluminium-based cohesive powders.

Finally, the experimental results of this work also show that another approach for powder flowability improvement lies in the application of heat treatment. With the cohesive Al-Cu powders tested in the present study, a precipitation hardening heat treatment allows to remove the residual humidity inside the powder as well as harden the particle, which results in a significant improvement in flowability. The impact

of heat treatment could be further analyzed through additional experiments, including the heat treatment of non heat-treatable cohesive aluminium powders (e.g. Al12Si), and testing the hardness of the powder bulk or individual particles before and after heat treatment. These additional experiments could more precisely uncover the relative importance of the effects of drying versus hardening in the improvement of powder flowability.

Acknowledgements

The results presented in this work were partially obtained in the context of project NENUFAR, which was sponsored by the Fonds Unique Interministériel of the Ministère de l'Economie et des Finances (France).

Bibliography

Aboulkhair, N. T., Everitt, N. M., Ashcroft, I., and Tuck, C. (2014). "Reducing porosity in AlSi10Mg parts processed by selective laser melting." *Additive Manufacturing*, Elsevier B.V., 1, 77–86.

Bergström, L. (1997). "Hamaker constants of inorganic materials." *Advances in Colloid and Interface Science*, 70, 125–169.

Capece, M., Ho, R., Strong, J., and Gao, P. (2015). "Prediction of powder flow performance using a multi-component granular Bond number." *Powder Technology*, Elsevier B.V., 286, 561–571.

Capece, M., Huang, Z., To, D., Aloia, M., Muchira, C., Davé, R. N., and Yu, A. B. (2014). "Prediction of porosity from particle scale interactions: Surface modification of fine cohesive powders." *Powder Technology*, 254, 103–113.

Capece, M., Silva, K. R., Sunkara, D., Strong, J., and Gao, P. (2016). "On the relationship of inter-particle cohesiveness and bulk powder behavior: Flowability of pharmaceutical powders." *International Journal of Pharmaceutics*, Elsevier B.V., 511(1), 178–189.

Carson, J. W., and Pittenger, B. H. (1998). "Bulk Properties of Powders." *Powder Metal Technologies and Applications*, ASM Handbook, 287–301.

Castellanos, A. (2005). "The relationship between attractive

interparticle forces and bulk behaviour in dry and uncharged fine powders." *Advances in Physics*, 54(4), 263–376.

Chen, Y., Yang, J., Dave, R. N., and Pfeffer, R. (2008). "Fluidization of coated group C powders." *AIChE Journal*, 54(1), 104–121.

CIRAL et al. (1996). "Advanced Aluminium Precision Casting for Integrally Stiffened Net-Shape Components (ADVACAST)." *European Community Project – BRITE/EURAM Programme*, CIRAL – Thyssen FeinguB – Mirtec S.A. – University of Lisboa – Technische Universität München – University of Patras.

Dumant, X. (1996). "Choix d'alliages de fonderie pour applications moteurs aéronautiques." *Internal Report*, Howmet CIRAL (ALCOA).

Dunst, P., Bornmann, P., Hemsel, T., and Sextro, W. (2018). "Vibration-Assisted Handling of Dry Fine Powders." *Actuators*, 7(2), 18.

Götzinger, M., and Peukert, W. (2003). "Dispersive forces of particle-surface interactions: Direct AFM measurements and modelling." *Powder Technology*, 130(1–3), 102–109.

Hascoët, J.-Y., Touzé, S., and Rauch, M. (2018). "Automated identification of defect geometry for metallic part repair by an additive manufacturing process." *Welding in the World*, 62(2), 229–241.

Hatch, J. E. (1984). *Aluminum Properties and Physical Metallurgy*. ASM International.

Huang, Z., Scicolone, J. V., Gurumuthy, L., and Davé, R. N. (2015). "Flow and bulk density enhancements of pharmaceutical powders using a conical screen mill: A continuous dry coating device." *Chemical Engineering Science*, Elsevier, 125, 209–224.

Israelachvili, J. N. (2011). *Intermolecular and Surface Forces*. Elsevier Inc.

Jiang, K., and Pinchuk, P. (2016). "Temperature and size-dependent Hamaker constants for metal nanoparticles." *Nanotechnology*, IOP Publishing, 27(34), 1–9.

Kerninon, J., Mognol, P., Hascoët, J.-Y., and Legonidec, C. (2008). "Effect of path strategies on metallic parts manufactured by additive process." *Solid Freeform Fabrication Symposium*, 352–361.

Laitinen, O., Bauer, K., Niinimäki, J., and Peuker, U. A. (2013). "Validity of the Rumpf and the Rabinovich adhesion force models for alumina substrates with nanoscale roughness." *Powder Technology*, Elsevier B.V., 246, 545–552.

LaMarche, C. Q., Leadley, S., Liu, P., Kellogg, K. M., and Hrenya, C. M. (2017). "Method of quantifying surface roughness for accurate adhesive force predictions." *Chemical Engineering Science*, Elsevier, 158(July 2016), 140–153.

LaMarche, C. Q., Miller, A. W., Liu, P., and Hrenya, C. M. (2016). "Linking micro-scale predictions of capillary forces to macro-scale fluidization experiments in humid environments." *AIChE Journal*, 62(10), 3585–3597.

Lefèvre, G., and Jolivet, a. (2009). "Calculation of Hamaker constants applied to the deposition of metallic oxide particles at high temperature." *Proceedings of International Conference on Heat Exchanger Fouling an Cleaning VIII*, 2009, 120–124.

Leite, F. L., Bueno, C. C., Da Róz, A. L., Ziemath, E. C., and Oliveira, O. N. (2012). "Theoretical models for surface forces and adhesion and their measurement using atomic force microscopy." *International Journal of Molecular Sciences*, 13(10), 12773–12856.

Liu, P., LaMarche, C. Q., Kellogg, K. M., and Hrenya, C. M. (2016). "Fine-particle defluidization: Interaction between cohesion, Young's modulus and static bed height." *Chemical Engineering Science*, Elsevier, 145, 266–278.

Matsusaka, S., Maruyama, H., Matsuyama, T., and Ghadiri, M. (2010). "Triboelectric charging of powders: A review." *Chemical Engineering Science*, Elsevier, 65(22), 5781–5807.

Muller, P., Mognol, P., and Hascoet, J. Y. (2013). "Modeling and control of a direct laser powder deposition process for Functionally Graded Materials (FGM) parts manufacturing." *Journal of Materials Processing Technology*, Elsevier B.V., 213(5), 685–692.

Osborne-Lee, I. W. (1988). "Calculation of Hamaker Coefficients for Metallic Aerosols from Extensive Optical Data." *Particles on Surfaces 1*, Springer US, Boston, MA, 77–90.

Planchamp, C., Carlier, P., and Dumant, X. (1993). "Etude de l'amélioration de la technique de coulée cire perdue procédé SOPHIA de pièces à parois minces en AU5MVZr." *Programme de développement STPA-CIRAL*, Howmet CIRAL - Pechiney, Marché STPA n°8996025004717586.

Polizzi, M. A., Franchville, J., and Hilden, J. L. (2016). "Assessment and predictive modeling of pharmaceutical powder flow behavior in small-scale hoppers." *Powder Technology*, Elsevier B.V., 294, 30–42.

Shah, U. V., Karde, V., Ghoroi, C., and Heng, J. Y. Y. (2017). "Influence of particle properties on powder bulk behaviour and processability." *International Journal of Pharmaceutics*, Elsevier B.V., 518(1–2), 138–154.

Spierings, A. B., Voegtlin, M., Bauer, T., and Wegener, K. (2015). "Powder flowability characterisation methodology for powder-bed-based metal additive manufacturing." *Progress in Additive Manufacturing*, Springer International Publishing, 1(1–2), 9–20.

Stichel, T., Laumer, T., Baumüller, T., Amend, P., and Roth, S. (2014). "Powder layer preparation using vibration-controlled

capillary steel nozzles for additive manufacturing." *Physics Procedia*, Elsevier B.V., 56(C), 157–166.

Stichel, T., Laumer, T., Linnenweber, T., Amend, P., and Roth, S. (2016). "Mass flow characterization of selective deposition of polymer powders with vibrating nozzles for laser beam melting of multi-material components." *Physics Procedia*, 83, 947–953.

Tan, J. H., Wong, W. L. E., and Dalgarno, K. W. (2017). "An overview of powder granulometry on feedstock and part performance in the selective laser melting process." *Additive Manufacturing*, Elsevier B.V., 18, 228–255.

Touzé, S., Rauch, M., and Hascoët, J.-Y. (2018). "Segmentation method for automated repair with an additive manufacturing process." *Conférence MUGV2018 & Manufacturing'21*, ENSAM ParisTech, Campus Bordeaux-Talence.

Touzé, S., Rauch, M., and Hascoët, J.-Y. (2019). "Design of powder projection nozzle for cohesive powder." France.

Vock, S., Klöden, B., Kirchner, A., Weißgärber, T., and Kieback, B. (2019). "Powders for powder bed fusion: a review." *Progress in Additive Manufacturing*, Springer International Publishing.

Yang, S., and Evans, J. R. G. (2005). "Acoustic initiation of powder flow in capillaries." *Chemical Engineering Science*, 60(2), 413–421.

Yang, S., and Evans, J. R. G. (2007). "Metering and dispensing of powder; the quest for new solid freeforming techniques." *Powder Technology*, 178(1), 56–72.